8156 *J. Phys. Chem. A* **2002,** *106,* 8156−8166

Theoretical Study on the Mechanism of the ^{1}CHCl + N_2O Reaction

Jian-jun Liu, Ji-kang Feng,* Hong Chen, Yi-hong Ding, and Chia-chung Sun

State Key Laboratory of Theoretical and Computational Chemistry, Jilin University, Changchun, Jilin 130023, Peoples' Republic of China

Received: March 5, 2002

The complex singlet potential energy surface of the $CHClN_2O$ system is investigated at the QCISD(T)/6-311G(d,p)//B3LYP/6-31G(d,p) level to explore the possible reaction mechanism of ^{1}CHCl radical with N_2O. Thirty minimum isomers and 56 transition states are located. In various possible initial association ways, the end-N attack leading to HClCNNO $\mathbf{a_1}$ is the most feasible pathway with the barrier of 8.9 kcal/mol. Starting from $\mathbf{a_1}$, the most feasible pathway is the direct cleavage of N−N bond leading to $\mathbf{P_1}$ HClCN + NO or to undergo a concerted Cl-shift and N−N bond cleavage to form $\mathbf{P_2}$ HCN + ClNO, both of which have a comparable contribution. In addition, $\mathbf{a_1}$ can isomerizate to HClCNNO $\mathbf{a_2}$ ($\mathbf{a_3}$) followed by the rupture of N−N bond to form $\mathbf{P_1}$. Furthermore, the primary products $\mathbf{P_1}$ and $\mathbf{P_2}$ further dissociate to the same product $\mathbf{P_{16}}$ HCN + NO + Cl. Much less competitively, $\mathbf{a_3}$ can alternatively undergo a ring-closure process leading to HCl-c(CNNO) **b** followed by the dissociation to product $\mathbf{P_3}$ N_2 + HClCO. The secondary dissociation of $\mathbf{P_3}$ may form the final product $\mathbf{P_{10}}$ N_2 + HCl + CO. The least favorable pathway should be that isomer $\mathbf{a_2}$ undergoes a concerted H-migration and N−N bond rupture to form product $\mathbf{P_4}$ ClCN + HNO. The similarities and discrepancies among the ^{1}CHX + N_2O (X = H, F, and Cl) reactions are discussed in terms of the substitution effect and the electronegativity of halogen atom. The present paper may assist in future experimental identification of the product distributions for the title reaction and may be helpful for understanding the halocarbene chemistry.

1. Introduction

Halocarbenes in the gas phase have attracted extensive attention of both experimental and theoretical chemists mainly due to their role in destroying ozone layer in stratosphere[1] and etching of semiconductor material.[2] As the simplest chlorocarbene, CHCl can be produced by the photoysis of the long-lived and abundant chloroform ($CHCl_3$) in stratosphere.[3−5] On the other hand, CHCl is also an important intermediate in the incineration of chlorine-containing wastes.[6] Under this condition, N_2O is inevitable to be produced. Particularly, it is known to be an intermediate in the conversion in flames of fuel-N and atmospheric N_2 to harmful pollutant NO.[7] For the investigation of CHCl + N_2O reaction, it is helpful to evaluate its role in combustion processes, since the title reaction may lead to two kinds of opposite products. One is NO and halogen-contained pollutants which are expected to be reduced, the other is atmospheric N_2.

In the last two decades, the studies of the reactivities for halocarbenes with some partners have been the important topic due to the role of inhibition. Experimentally, the reaction rates or reactivities of halocarbenes with some species N, O, H_2, O_2, NO, N_2O, NO_2, CH_4, and unsaturated hydrocarbons, have been studied.[8−21] Fernandez et al. measured the total reaction rate of CHF + N_2O reaction to be $(2.55 \pm 0.15) \times 10^{-12}$ cm^{3}molecule^{-1}s^{-1}.[19] In addition, the reactions of CHCl with NO and NO_2 have been the subject of experimental investigations.[20,21] Theoretically, the potential energy surfaces of CHX + NO (X = H, F, Cl) reactions have been built up.[22−27] The total rate constants may increase along X = F, Cl, and H with the decreased electronegativity. On the other hand, the feasibility order of the C−X bond cleavage in HXCNO or X-shift in an important processes HXCNO→c−C(HX)NO →HNC(X)O or XNC(H)O (X = H, F, Cl) is consistent with the decreased C−X bond enthalpies along X = F, H, and Cl. As a result, the CHCl + NO reaction represents a better model of CHBr + NO and CHI + NO reaction than the CHF + NO reaction, both of which may play an important role in reducing pollutants and for which the accurate experimental data are difficult to obtain.[20] Similarly, whether the similar situation would exist in ^{1}CHX + N_2O reaction system or not till waits to be tested.

Very recently, we have initiated a series of potential energy surfaces (PES) on ^{1}CHX + N_2O (X = H, F, Cl) reactions. The potential energy surfaces of $^1CH_2$ + N_2O [28] and ^{1}CHF + N_2O[29] reactions were calculated at the QCISD(T)/6-311G(d,p)//B3LYP/6−31 G(d,p) level. The features of the potential energy surfaces of two reactions are almost in parallel. However, some quantitative discrepancy leads to the different product distribution for the two reactions. Then, the question arises: in terms of the product distribution, is ^{1}CHCl + N_2O similar to $^1CH_2$ + N_2O or to ^{1}CHF + N_2O?

To the best of our knowledge, no experimental and theoretical studies have been reported for the title reaction. Therefore, it is highly desirable to carry out the detailed theoretical study on the PES of the title reaction. The main objectives of the present paper are to (1) provide the detailed isomerization and dissociation channels on the $CHClN_2O$ PES; (2) determine the product distribution of ^{1}CHCl + N_2O reaction to assist in future experimental identification; (3) make comparisons between the CHX (X = F, Cl, H) reactions with N_2O in order to deeply understand the halocarbene chemistry.

2. Computational Methods

All calculations are carried out using the Gaussian 98 program.[30] The geometries of all the reactants, products, various intermediates, and transition states for the ^{1}CHCl + N_2O reaction

10.1021/jp020623u CCC: $22.00

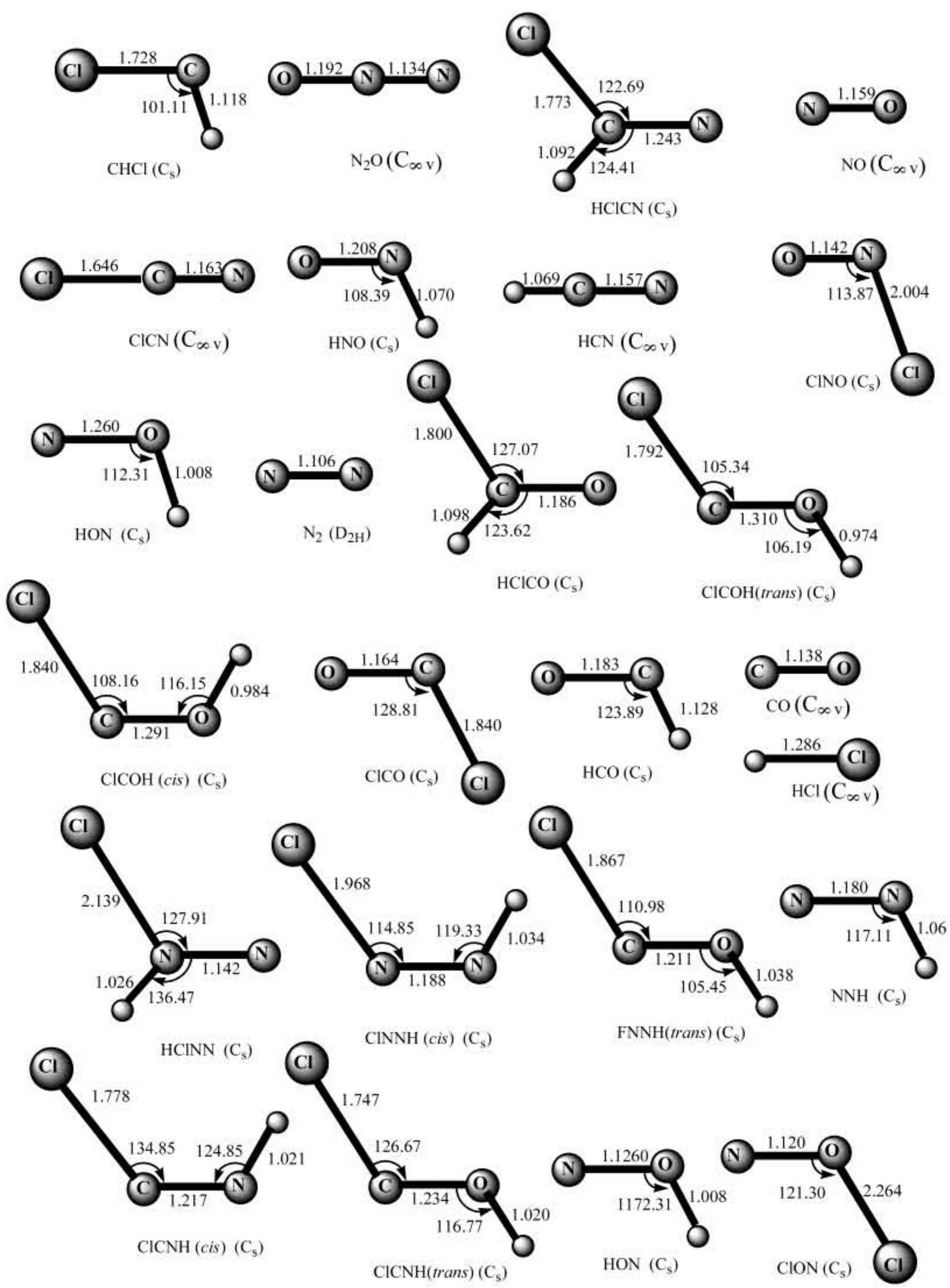

Figure 1. B3LYP/6-31G(d,p)-optimized geometries of reactants and products. Bond distances are in angstroms and angles are in degrees.

are optimized using hybrid density functional B3LYP method with the 6-31G(d,p) basis set. Vibrational frequencies are calculated at the B3LYP/6-31G(d,p) level to check whether the obtained stationary points correspond to isomers or to first-order transition states. To confirm that the transition state connect designated intermediates, we also perform intrinsic reaction coordinate (IRC) calculations at the B3LYP/6-31G(d,p) level. In addition, single point energies are calculated for the B3LYP/6-31G(d,p) optimized geometries with the quadratic configuration interaction method with single and double excitation and perturbative corrections for triple excitations (QCISD(T)) with the 6-311G(d,p) basis set. Unless otherwise specified, the QCISD(T) single-point energies are used in the following discussions.

3. Results and Discussions

Starting from the reactants **R** ^{1}CHCl + N_2O, fifteen energetically accessible primary products ($\mathbf{P_1}$−$\mathbf{P_{15}}$) of the title reaction are considered in this paper. In addition, four secondary dissociation products $\mathbf{P_{16}}$−$\mathbf{P_{19}}$ from the relevant primary products $\mathbf{P_1}$, $\mathbf{P_2}$, $\mathbf{P_3}$, and $\mathbf{P_4}$ also are included. Figure 1 shows the optimized geometries of the reactants and products. The energetic data of the reactants and all products are listed in Table 1. For the present ^{1}CHCl + N_2O reaction, thirty intermediate isomers (denoted by the letters from **a** to **p**) including twenty-six open-chain and four cyclic species are located at the B3LYP/6-31G(d,p) level. To ascertain the interrelation between various isomers and dissociation products, fifty-six transition states are

TABLE 1: Zero-Point, Total (a.u.), and Relative Energies in Parentheses (kcal/mol) as Well as Those Including Zero-Point Vibration Energies (kcal/mol) of Reactants and Products for the ^{1}CHCl + N$_2$O Reaction

species	ZPE	B3LYP	QCISD(T)	QCISD(T) + ZPE
R ^{1}CHCl + N$_2$O	14.1	−683.422486 (0.0)	−682.425132 (0.0)	0.0
P$_1$ HClCN + NO	14.1	−683.468446 (−28.8)	−682.470366 (−28.4)	−28.3
P$_2$ HCN + ClNO	14.4	−683.509791 (−54.8)	−682.513806 (−55.6)	−55.2
P$_3$ N$_2$ + HClCO	15.6	−683.642538 (−138.1)	−682.654913 (−144.2)	−142.7
P$_4$ ClCN + HNO	14.2	−683.478974 (−35.4)	−682.489160 (−40.2)	−40.0
P$_5$ N$_2$ + ClCOH(c)	14.8	−683.564968 (−89.4)	−682.577793 (−95.8)	−95.0
P$_6$ N$_2$ + ClCOH(t)	15.2	−683.564451 (−89.1)	−682.579745 (−97.0)	−95.9
P$_7$ CO + HClNN	14.7	−683.530090 (−67.5)	−682.539994 (−42.1)	−71.5
P$_8$ CO + HNNCl(c)	14.7	−683.539294 (−73.3)	−682.547175 (−76.6)	−75.9
P$_9$ CO + HNNCl(t)	14.8	−683.533146 (−69.4)	−682.542322 (−73.5)	−72.8
P$_{10}$ N$_2$ + HCl + CO	10.9	−683.634360 (−133.0)	−682.668374 (−152.6)	−155.8
P$_{11}$ ClCO + N$_2$H	12.4	−683.496687 (−46.6)	−682.494922 (−43.8)	−45.4
P$_{12}$ NO + ClCNH(c)	14.0	−683.456303 (−21.2)	−682.456409 (−19.6)	−19.7
P$_{13}$ NO + ClCNH(t)	14.4	−683.461353 (−24.4)	−682.462493 (−23.4)	−23.1
P$_{14}$ HON + ClCN	13.8	−683.413822 (5.4)	−682.419741 (3.4)	3.1
P$_{15}$ ClON + HCN	14.3	−683.466707 (−27.7)	−682.476198 (−32.0)	−31.8
P$_{16}$ NO + HCN + Cl	13.2	−683.448993 (−16.6)	−682.465750 (−25.5)	−39.5
P$_{17}$ NO + ClCN + H	8.4	−683.396725 (16.2)	−682.413150 (7.5)	1.8
P$_{18}$ N$_2$ + HCO + Cl	11.7	−683.512215 (−56.3)	−682.531085 (−66.5)	−68.8
P$_{19}$ N$_2$ + ClCO + H	7.6	−683.488363 (−41.3)	−682.506828 (−51.3)	−57.7

located, which are denoted as the symbols "**TSxy**". For example, **TSa$_3$b** denotes the transition state connecting the isomers **a$_3$** and **b**. The optimized structures of the intermediates and transition states are shown in Figures 2 and 3, respectively. Tables 2 and 3 list the energies of the intermediates and transition states, respectively. The reaction pathways related to the singlet [CHClN$_2$O] potential energy surface (PES) are schematically plotted in Figure 4, parts a, b, and c.

3.1 Initial Association. The attack of the singlet CHCl at N$_2$O molecule may have five possible ways, i.e., end-N attack, end-O attack, middle-N attack, side N−N π bonding attack, and side N−O π bonding attack. The end-N attack can form chainlike isomer HClCNNO **a** (**a$_1$**, **a$_2$**, **a$_3$**). We locate the addition transition state **TSRa$_1$** linking the reactants **R** to **a$_1$** using the HF, MP2, B3LYP methods with 6-31G(d,p) basis set. It is worth comparing the calculated results at the various theory levels. In terms of structure and energy, B3LYP-calculated results are in good agreement with MP2-calculated one, whereas HF-calculated results differ from the other two. Thus, it is very necessary to perform the calculation including the correction of the correlation energy for the title reaction. Both end-O and side N−O π bonding attacks directly lead to the same product **P$_3$** N$_2$ + HClCO via the transition states **TSRP$_3$-O** and **TSRP$_3$-NO**, which lie 16.6 and 19.3 kcal/mol higher than the reactants **R**, respectively. The other considerable barrier-consumed process is side N−N π bonding attack leading to three-membered ring isomer HCl-c(CNN)O **j**. The transition state **TSRj** is 19.1 kcal/mol higher than the reactants **R**. As shown in Figure 4 (a), **j** is readily to isomerizate to end-N adduct **a$_2$** through the ring-open transition state **TSa$_2$j**. Such a process only requires overcoming 19.3 kcal/mol barrier relative to **j**. On the other hand, it is impossible to take place for the further isomerization and dissociation leading to ClCN(O)NH **k** and **P$_3$** N$_2$ + HClCO from **j**, since the transition states **TSjk** and **TSjP$_3$** are 31.4 and 18.8 kcal/mol higher than the reactants **R**. Therefore, the formation of **j** is unlikely important for the total reaction. We try to optimize the adduct of middle-N attack to form HClCN(O)N, yet with no success. Such a search usually leads to **a** or **j**. In conclusion, end-N attack leading to **a$_1$** is energetically the most feasible way. In the following discussions, we mainly discuss the formation pathways of various products proceeded via **a$_1$**.

Starting from HClCNNO **a$_1$**, various products can be formed via successive isomerization and dissociation pathways. In the following parts, we will first discuss the formation pathways of the four kinetically feasible primary products **P$_1$** HClCN + NO, **P$_2$** HCN + ClNO, **P$_3$** N$_2$ + HClCO, and **P$_4$** ClCN + HNO. Further, we will also discuss the secondary dissociation pathways of these four primary products. Finally, the unfeasible product channels are also considered.

3.2 Reaction Pathways. *3.2.1 P$_1$HClCN + NO, **P$_2$** HCN + ClNO, **P$_3$** N$_2$ + HClCO, and **P$_4$** ClCN + HNO.* The initially formed end-N attack isomer HClCNNO **a** can directly dissociate to the product **P$_1$** HFCN + NO via the N−N single bond rupture. Such a simple process can be depicted as

Path1 P$_1$: **R** ^{1}CHCl + N$_2$O→*trans*-HClCNNO **a$_1$**→**P$_1$** HClCN + NO

Path2 P$_1$: **R** ^{1}CHCl + N$_2$O→*trans*-HClCNNO **a$_1$**→*trans*-HClCNNO **a$_2$**→**P$_1$** HClCN + NO

Despite numerous attempts, optimization of any transition structures from **a** to **P$_1$** often leads to product **P$_1$** or **a** at the B3LYP/6-31G(d,p) level. At the MP2/6-31G(d,p) level, the transition states **TSa$_1$P$_1$** and **TSa$_2$P$_1$** are obtained. In **TSa$_1$P$_1$** and **TSa$_2$P$_1$**, the dissociating C−N bond distances have reached 2.938 and 2.841 Å, respectively, indicative of the character of "late" saddle point. However, single-point energy calculations show that **TSa$_1$P$_1$** and **TSa$_2$P$_1$** lie 1.1 and 2.3 kcal/mol lower than **P$_1$**, respectively. It shows that after surmounting the barriers of these two transition states, the very stable complexes might be formed followed by the dissociation to **P$_1$**. Note of the numerous optimizations of the transition state **TSa$_2$P$_1$** usually lead to product **P$_1$** or **TSa$_1$P$_1$** or **TSa$_3$P$_1$** at the MP2/6-31G-(d,p) level.

The isomer *trans*-HClCNNO **a$_1$** can also undergo a concerted Cl-shift and N−N bond rupture leading to product **P$_2$** HCN + ClNO. Similarly, *trans*-HClCNNO **a$_2$** can alternatively undergo a concerted H-shift and N−N bond cleavage to form product **P$_4$** ClCN + HNO via **TSa$_2$P$_4$**. The isomer *cis*-CHClN$_2$O **a$_3$** can take a ring-closure to form the four-membered ring intermediate HCl-c(CNNO) **b** followed by dissociation to product **P$_3$** N$_2$ +

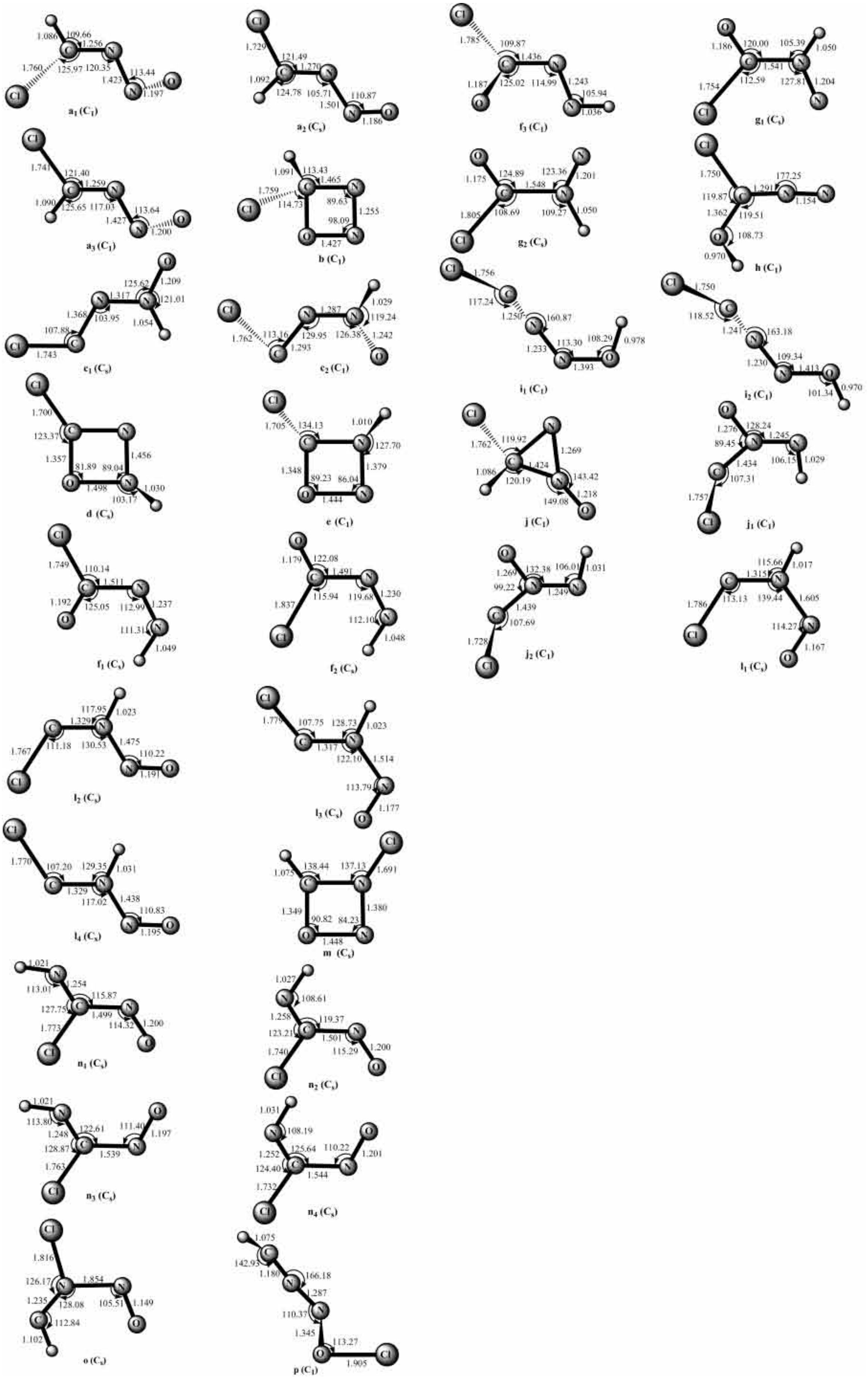

Figure 2. B3LYP/6-31G(d,p)-optimized geometries of all isomers. Bond distances are in angstroms and angles are in degrees.

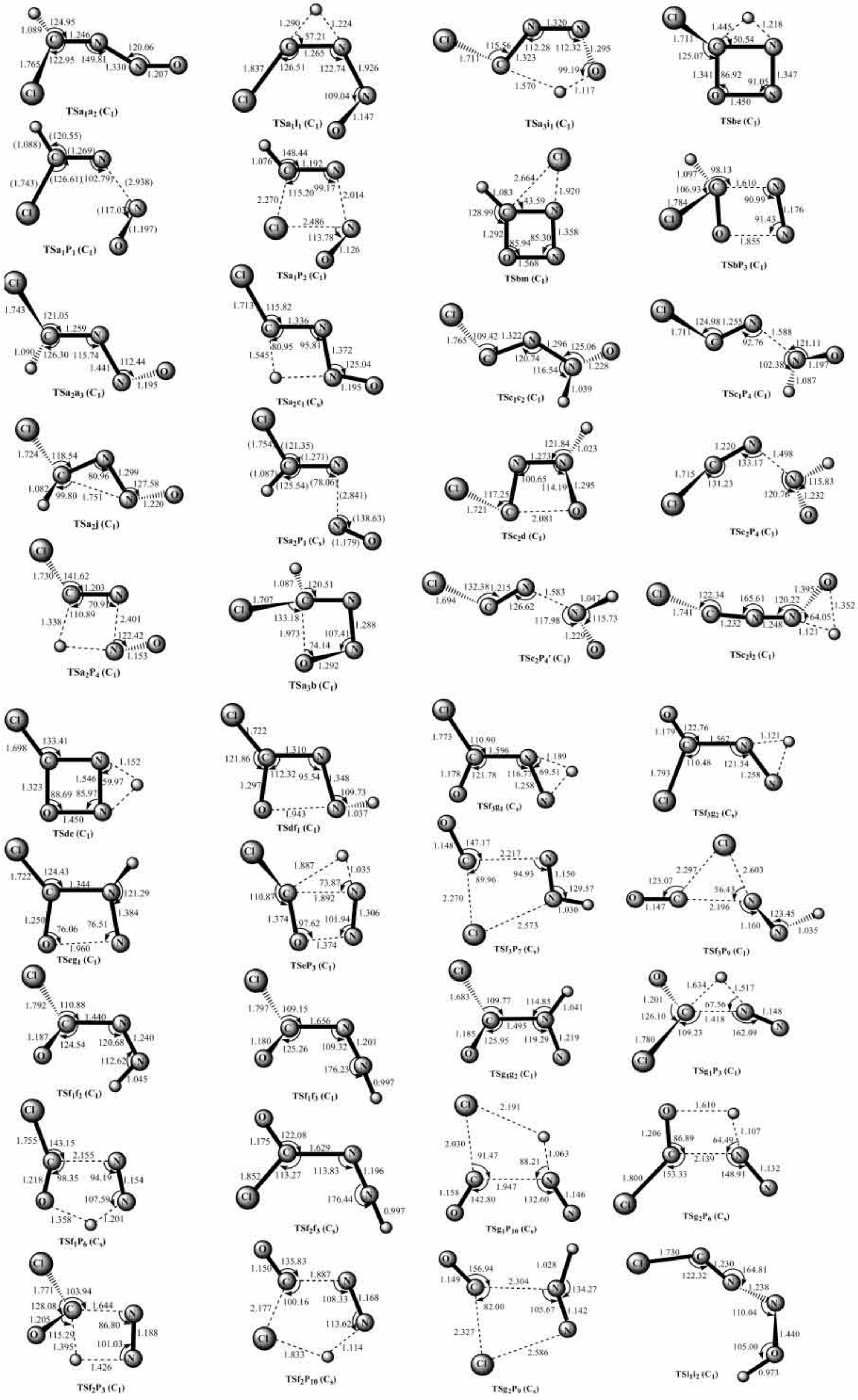

TSa_1a_2 (C_1) TSa_1i_1 (C_1) TSa_3i_1 (C_1) TSbe (C_1)

TSa_1P_1 (C_1) TSa_1P_2 (C_1) TSbm (C_1) TSbP_3 (C_1)

TSa_2a_3 (C_1) TSa_2c_1 (C_s) TSc_1c_2 (C_1) TSc_1P_4 (C_1)

TSa_2j (C_1) TSa_2P_1 (C_s) TSc_2d (C_1) TSc_2P_4 (C_1)

TSa_2P_4 (C_1) TSa_3b (C_1) TSc_2P_4' (C_1) TSc_2i_2 (C_1)

TSde (C_1) TSdf_1 (C_1) TSf_3g_1 (C_s) TSf_3g_2 (C_s)

TSeg_1 (C_1) TSeP_3 (C_1) TSf_3P_7 (C_s) TSf_3P_9 (C_1)

TSf_1f_2 (C_1) TSf_1f_3 (C_1) TSg_1g_2 (C_1) TSg_1P_3 (C_1)

TSf_1P_6 (C_s) TSf_2f_3 (C_s) TSg_1P_{10} (C_s) TSg_2P_6 (C_s)

TSf_2P_3 (C_1) TSf_2P_{10} (C_s) TSg_2P_9 (C_s) TSi_1i_2 (C_1)

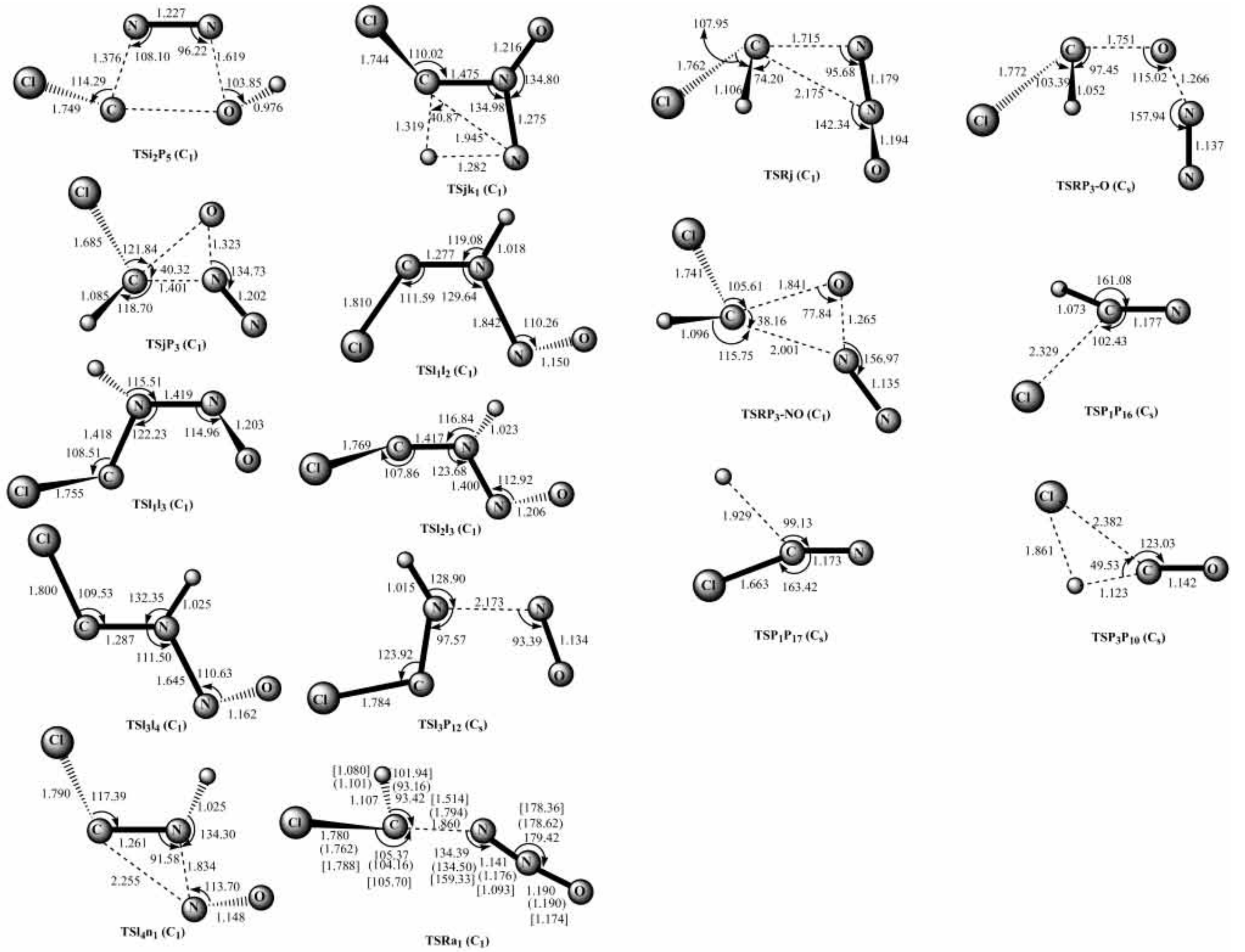

Figure 3. B3LYP/6-31G(d,p)-optimized geometries of all transition states. Bond distances are in angstroms and angles are in degrees. The MP2/6-31G(d,p) and HF/6-31G(d,p)-optimized geometries are also given in parentheses and square brackets, respectively.

HClCO. These product pathways can be written as

Path P_2: **R** ^{1}CHCl + N_2O→*trans*-HClCNNO **a_1**→**P_2** HCN + ClNO

Path P_3: **R** ^{1}CHCl + N_2O→***trans*-HClCNNO a_1**→*cis*-HClCNNO **a_3**→HCl-c(CNNO) **b**→**P_3** N_2 + HClCO

Path P_4: **R** ^{1}CHCl + N_2O→*trans*-HClCNNO**a_1**→*trans*-HClCNNO**a_2**→**P_4** ClCN + HNO

As shown in Figure 4a, in **Path P_1**, **Path P_2**, **Path P_3**, and **Path P_4**, all of the transition states and isomers lie below the reactants **R** except for the common transition state **TSRa$_1$**. As a result, **P_1**−**P_4** are favorable for the total reaction.

Subsequently, let us discuss the secondary dissociation reactions of the primary products **P_1** HClCN + NO, **P_2** HCN + ClNO, **P_3** N_2 + HClCO, and **P_4** ClCN + HNO. **P_1** can further dissociate to give **P_{16}** NO + HCN + Cl and **P_{17}** NO + ClCN + H via the direct C−Cl and C−H single bond rupture, respectively. In addition, **P_2** and **P_4** can further lead to **P_{16}** and **P_{17}** via the N−Cl and N−H single bond dissociation, respectively. For the N−H and N−Cl bond rupture processes, the well-defined transition states cannot be obtained at the B3LYP/6-31G(d,p) level. However, it is impossible to form **P_{17}** via **P_1** and **P_4** due to the thermodynamical and kinetic hinderences, whereas the formation pathway of **P_{16}** (via **P_1** and **P_2**) is feasible. As we can see in Figure 4a, there are three possible dissociation pathways for **P_3**. The most favorable pathway should be the formation of **P_{10}** N_2 + HCl + CO through the HCl-side elimination transition state **TSP$_3$P$_{10}$**. The barrier of 37.4 kcal/mol is needed to overcome. On the contrary, the formation of **P_{18}** N_2 + HCO + Cl and **P_{19}** N_2 + ClCO + H requires the endothermicity of 73.9 and 85.0 kcal/mol, respectively. Thus, we expect that the final product of **P_3** should be **P_{10}**, not **P_{18}** and **P_{19}**.

3.2.2 Other Products. Now, we turn to the other isomerization and dissociation channels of the isomers HClCNNO **a** and HCl-c(CNNO) **b**. First, we should consider the H-shift processes of these isomers. The isomers HClCNNO **a_1**, **a_2**, and **a_3** can undergo 1,3-H-shift, 1,2-H-shift, and 1,4-H-shift leading to chainlike isomers ClCNN(H)O **c_1**, $ClCN_2OH$ **i_1**, and ClCN(H)NO **l_1**, respectively. However, these conversion transition states **TSa$_1$c$_1$**, **TSa$_2$i$_1$**, and **TSa$_3$l$_1$** lie 7.4, 2.3, and 20.3 kcal/mol higher than the reactants **R**. The four-membered ring isomer HCl-c(CNNO) **b** can undergo 1,2-H-shift from C-atom to N-atom to give the other four-membered ring intermediate Cl-c(CN(H)NO) **e** via the transition state **TSbe** with the relative energy of 14.9 kcal/mol. Clearly, all these H-migration reaction pathways are not feasible for the ^{1}CHCl + N_2O reaction.

TABLE 2: Zero-Point, Total (a.u.), and Relative Energies in Parentheses (kcal/mol) as Well as Those Including Zero-Point Vibration Energies (kcal/mol) of Intermediates for the ^{1}CHCl + N$_2$O Reaction

species	ZPE	B3LYP	QCISD(T)	QCISD(T) + ZPE
$\mathbf{a}_1$	17.3	−683.510579 (−55.3)	−682.505056 (−50.2)	−46.9
$\mathbf{a}_2$	17.2	−683.509899 (−54.9)	−682.506507 (−51.1)	−47.9
$\mathbf{a}_3$	17.2	−683.507671 (−53.5)	−682.503359 (−49.1)	−46.0
b	18.6	−683.503846 (−51.1)	−682.501209 (−47.7)	−43.2
$\mathbf{c}_1$	17.8	−683.437981 (−9.7)	−682.429159 (−2.5)	1.2
$\mathbf{c}_2$	17.7	−683.439229 (−10.5)	−682.426164 (−0.6)	3.0
d	19.0	−683.494131 (−45.0)	−682.487710 (−39.3)	−34.3
e	18.3	−683.461738 (−24.6)	−682.451527 (−16.6)	−12.3
$\mathbf{f}_1$	18.1	−683.560993 (−86.9)	−682.559710 (−84.4)	−80.4
$\mathbf{f}_2$	17.9	−683.560945 (−86.9)	−682.557348 (−83.0)	−79.1
$\mathbf{f}_3$	18.2	−683.565020 (−89.4)	−682.563239 (−86.7)	−82.5
$\mathbf{g}_1$	17.6	−683.533619 (−69.7)	−682.526182 (−63.4)	−59.9
$\mathbf{g}_2$	17.4	−683.532187 (−68.3)	−682.524659 (−62.5)	−59.1
h	17.9	−683.530610 (−67.8)	−682.522518 (−61.1)	−57.3
$\mathbf{i}_1$	17.1	−683.457780 (−22.1)	−682.446801 (−13.6)	−10.6
$\mathbf{i}_2$	17.3	−683.463178 (−25.5)	−682.452716 (−17.3)	−14.0
j	18.5	−683.475443 (−33.2)	−682.467841 (−26.8)	−22.3
$\mathbf{k}_1$	17.2	−683.408510 (8.8)	−682.400158 (15.7)	18.9
$\mathbf{k}_2$	17.4	−683.413101 (5.9)	−682.405152 (12.5)	15.8
$\mathbf{l}_1$	16.4	−683.453888 (−19.7)	−682.449818 (−15.5)	−13.1
$\mathbf{l}_2$	16.9	−683.460053 (−23.6)	−682.456285 (−19.5)	−16.7
$\mathbf{l}_3$	16.8	−683.458899 (−22.8)	−682.456423 (−19.6)	−16.6
$\mathbf{l}_4$	17.0	−683.463880 (−26.0)	−682.460690 (−22.3)	−19.0
m	17.4	−683.418668 (2.4)	−682.406130 (11.9)	15.2
$\mathbf{n}_1$	17.8	−683.518568 (−60.3)	−682.515699 (−56.8)	−53.1
$\mathbf{n}_2$	17.8	−683.517113 (−59.4)	−682.515150 (−56.5)	−52.8
$\mathbf{n}_3$	17.3	−683.512086 (−56.2)	−682.510847 (−53.8)	−50.5
$\mathbf{n}_4$	17.6	−683.514287 (−57.6)	−682.513849 (−55.7)	−52.1
o	15.1	−683.413359 (5.7)	−682.406569 (11.6)	12.7
p	15.3	−683.405644 (10.6)	−682.383070 (26.4)	27.7

Therefore, though **c**, **e**, **i**, and **l** can further convert to the other isomers or the products $\mathbf{P_3}$ N$_2$ + HClCO, $\mathbf{P_4}$ ClCN + HNO, $\mathbf{P_5}$ N$_2$ + ClCOH(cis), $\mathbf{P_{12}}$ NO + ClCNH(cis), $\mathbf{P_{13}}$ NO + ClCNH-(trans), these processes are kinetically unfavorable.

On the other hand, we should also consider Cl-shift processes from **a** and **b**. The isomers HClCNNO $\mathbf{a_1}$, $\mathbf{a_2}$, and $\mathbf{a_3}$ can undergo a Cl-shift to form HCN(Cl)NO **o**, HCNN(Cl)O, and HCNNOCl **p**. Note that we cannot locate isomer HCNN(Cl)O at the B3LYP/6-31G(d,p) level. As shown in Table 2, **o** and **p** lie 12.7 and 27.7 kcal/mol above the reactants **R**, respectively. In addition, the four-membered ring isomer HCl-c(CNNO) **b** can undergo a 1,2-Cl-shift from C-atom to N-atom to form H−c(CN(Cl)NO) **m**. However, **TSbm** and **m** are 28.7 and 15.2 kcal/mol higher than **R**. All in all, Starting from **a** and **b**, all Cl-shift processes are both thermodynamically and kinetically unfeasible. Therefore, the further isomerization and dissociation of these processes are unimportant and then will not be considered.

It should be pointed out that the OCNN-framed isomers OC-(Cl)NNH **f** and OC(Cl)N(H)N **g** are very low-lying, as shown in Figure 4 (c). However, all of the reaction pathways leading to them involve the high-lying transition states that lie above the reactants **R**. The isomers **f** and **g** can lead to the complex products $\mathbf{P_3}$ N$_2$ + HClCO, $\mathbf{P_6}$ N$_2$ + ClCOH (trans), $\mathbf{P_9}$ CO + HNNCl(trans), $\mathbf{P_{10}}$ N$_2$ + HCl + CO, and $\mathbf{P_{11}}$ ClCO + N$_2$H. Though the dissociation transition states from **f** or **g** lie below the reactants **R**, the formation pathways of these products are kinetically unfeasible for the title reaction.

3.3 Reaction Mechanism. In Section 3.2, we have obtained several important reaction channels that are both thermodynamically and kinetically accessible for the ^{1}CHCl + N$_2$O reaction. Note that the feasible secondary dissociation pathways are also included. Here, for ease of discussion, they are listed again

Path1 $\mathbf{P_1}$: R ^{1}CHCl + N$_2$O→*trans*-HClCNNO $\mathbf{a_1}$→$\mathbf{P_1}$ HClCN + NO

Path2 $\mathbf{P_1}$: R ^{1}CHCl + N$_2$O→*trans*-HClCNNO $\mathbf{a_1}$→*trans*-HClCNNO $\mathbf{a_2}$→$\mathbf{P_1}$ HClCN + NO

Path $\mathbf{P_2}$: **R** ^{1}CHCl + N$_2$O→*trans*-HClCNNO $\mathbf{a_1}$→$\mathbf{P_2}$ HCN + ClNO

Path $\mathbf{P_3}$: **R** ^{1}CHCl + N$_2$O→***trans*-HClCNNO** $\mathbf{a_1}$→*cis*-HClCNNO $\mathbf{a_3}$→HCl-c(CNNO) **b**→$\mathbf{P_3}$ N$_2$ + HClCO

Path $\mathbf{P_4}$: **R** ^{1}CHCl + N$_2$O→*trans*-HClCNNO $\mathbf{a_1}$→*trans*-HClCNNO $\mathbf{a_2}$→$\mathbf{P_4}$ ClCN + HNO

All of them are schematically shown in Figure 4a. We can find easily that all reaction pathways involve the chainlike isomer HClCNNO $\mathbf{a_1}$. Starting form $\mathbf{a_1}$, the least competitive pathway should be **Path $\mathbf{P_4}$** because $\mathbf{TSa_1P_4}$ (−11.4) lies more higher than $\mathbf{TSa_1P_1}$ (−26.0) in **Path2 $\mathbf{P_1}$**, $\mathbf{TSa_2P_1}$ (−27,2) in **Path1 $\mathbf{P_1}$**, $\mathbf{TSa_1P_2}$ (−28.6) in **Path $\mathbf{P_2}$**, and $\mathbf{TSa_3b}$ (−17.1) in **Path $\mathbf{P_3}$**. Further, the relative energy of $\mathbf{TSa_3b}$ in **Path $\mathbf{P_3}$** is higher than those of $\mathbf{TSa_1P_1}$ in **Path1 $\mathbf{P_1}$**, $\mathbf{TSa_2P_1}$ in **Path2 $\mathbf{P_1}$** and $\mathbf{TSa_1P_2}$ in **Path $\mathbf{P_2}$**. Thus, we expect that **Path $\mathbf{P_3}$** cannot compete with **Path1 $\mathbf{P_1}$**,**Path2 $\mathbf{P_1}$** and **Path $\mathbf{P_2}$**. In addition, the formation of $\mathbf{P_1}$ via **Path2 $\mathbf{P_1}$** requires surmounting two barriers, whereas for **Path1 $\mathbf{P_1}$** and **Path $\mathbf{P_2}$**, each involves only one moderately high barrier. As a result, **Path2 $\mathbf{P_1}$** has a lower

TABLE 3: Zero-Point, Total (a.u.), and Relative Energies in Parentheses (kcal/mol) as Well as Those Including Zero-Point Vibration Energies (kcal/mol) of Transition States for the ^{1}CHCl + N$_2$O Reaction

species	ZPE	B3LYP	QCISD(T)	QCISD(T) + ZPE
TSa$_1$a$_2$	16.9	−683.494211 (−45.0)	−682.478222 (−33.3)	−30.5
TSa$_1$l$_1$	12.3	−683.392404 (18.9)	−682.390028 (22.0)	20.3
[b]**TSa$_1$P$_1$**	15.0	−682.284752 (−25.3)	−682.468100 (−27.0)	−26.0
TSa$_1$P$_2$	15.8	−683.481562 (−37.1)	−682.473586 (−30.4)	−28.6
TSa$_2$a$_3$	16.9	−683.507501 (−53.3)	−682.503344 (−49.1)	−46.2
TSa$_2$c$_1$	14.9	−683.424538 (−1.3)	−682.414681 (6.6)	7.4
TSa$_2$j	17.0	−683.443354 (−13.1)	−682.434557 (−5.9)	−3.0
[b]**TSa$_2$P$_1$**	15.5	−682.287068 (−26.7)	−682.470768 (−28.6)	−27.2
TSa$_2$P$_4$	13.3	−683.441817 (−12.1)	−682.442085 (−10.6)	−11.4
TSa$_3$b	17.4	−683.464969 (−26.7)	−682.457711 (−20.4)	−17.1
TSa$_3$i$_1$	14.9	−683.432960 (−6.6)	−682.422803 (1.5)	2.3
TSbe	15.4	−683.411158 (7.1)	−682.403617 (13.5)	14.9
TSbm	16.5	−683.399448 (14.5)	−682.383214 (26.3)	28.7
TSbP$_3$	16.7	−683.475341 (−33.2)	−682.471564 (−29.1)	−26.5
TSc$_1$c$_2$	17.2	−683.431161 (−5.4)	−682.419519 (3.5)	6.6
TSc$_1$P$_4$	15.6	−683.418507 (2.5)	−682.412838 (7.7)	9.3
TSc$_2$d	17.4	−683.421090 (0.9)	−682.409878 (9.6)	13.0
TSc$_2$i$_2$	13.7	−683.362253 (37.8)	−682.346101 (50.0)	49.2
TSc$_2$P$_4$	16.4	−683.423414 (−0.6)	−682.414767 (6.5)	8.8
TSc$_2$P$_4$′	16.2	−683.419109 (2.1)	−682.411414 (8.6)	10.7
TSde	15.6	−683.414258 (5.2)	−682.406784 (11.5)	13.0
TSdf$_1$	17.5	−683.466906 (−27.9)	−682.460669 (−22.3)	−18.8
TSeg$_1$	16.7	−683.432443 (−6.2)	−682.421702 (2.2)	4.8
TseP$_3$	16.3	−683.386931 (22.3)	−682.381924 (27.1)	29.5
TSf$_1$f$_2$	17.8	−683.557353 (−84.6)	−682.554603 (−81.2)	−77.5
TSf$_1$f$_3$	15.9	−683.490421 (−42.6)	−682.482283 (−35.9)	−34.0
TSf$_1$P$_6$	14.6	−683.525127 (−64.4)	−682.520335 (−59.7)	−59.2
TSf$_2$f$_3$	15.9	−683.494876 (−45.4)	−682.485673 (−38.0)	−36.2
TSf$_2$P$_3$	14.2	−683.456196 (−21.2)	−682.454736 (−18.6)	−18.4
TSf$_2$P$_{10}$	15.3	−683.542636 (−75.4)	−682.539280 (−71.6)	−70.4
TSf$_3$g$_1$	13.9	−683.448857 (−16.5)	−682.446180 (−13.2)	−13.4
TSf$_3$g$_2$	14.1	−683.453316 (−19.3)	−682.449338 (−15.2)	−15.2
TSf$_3$P$_7$	15.5	−683.505075 (−51.8)	−682.502040 (−48.3)	−46.8
TSf$_3$P$_9$	14.9	−683.488590 (−41.5)	−682.483420 (−36.6)	−35.8
TSg$_1$g$_2$	17.1	−683.520566 (−61.5)	−682.514054 (−55.8)	−52.8
TSg$_1$P$_3$	14.0	−683.460934 (−24.1)	−682.455129 (−18.8)	−18.8
TSg$_1$P$_{10}$	15.7	−683.522059 (−62.5)	−682.514049 (−55.8)	−54.1
TSg$_2$P$_6$	14.8	−683.506870 (−53.0)	−682.499789 (−46.8)	−45.9
TSg$_2$P$_9$	15.2	−683.499171 (−48.1)	−682.495918 (−44.4)	−43.3
TSi$_1$i$_2$	16.5	−683.451408 (−18.1)	−682.442370 (−10.8)	−8.4
TSi$_2$P$_5$	15.9	−683.417952 (2.8)	−682.409286 (9.9)	11.7
TSjk$_1$	14.8	−683.381029 (26.0)	−682.376265 (30.7)	31.4
TSjP$_3$	16.5	−683.398680 (14.9)	−682.399154 (16.3)	18.8
TSl$_1$l$_2$	15.8	−683.449122 (−16.7)	−682.445781 (−13.0)	−11.2
TSl$_1$l$_3$	15.6	−683.411327 (7.0)	−682.404427 (13.0)	14.5
TSl$_2$l$_4$	15.4	−683.409853 (7.9)	−682.401656 (14.7)	16.1
TSl$_3$l$_4$	15.8	−683.445105 (−14.2)	−682.444288 (−12.0)	−10.3
TSl$_3$P$_{12}$	16.1	−683.448702 (−16.5)	−682.447851 (−14.3)	−12.2
TSl$_4$n	15.8	−683.445992 (−14.8)	−682.438208 (−8.2)	−6.5
TSRa$_1$	17.8[a]	−681.442899[a](22.9)	−682.406306 (8.1)	10.6
	16.1[b]	−682.239344[b](3.2)	−682.410943 (7.7)	9.8
	15.8	−683.419915 (1.6)	−682.413866 (7.1)	8.9
TSRj	15.7	−683.406271 (10.2)	−682.397246 (17.5)	19.1
TSRP$_3$-O	15.4	−683.408347 (8.9)	−682.400794 (15.3)	16.6
TSRP$_3$-NO	15.8	−683.404838 (11.1)	−682.397171 (17.5)	19.3
TSP$_1$P$_{16}$ + NO	13.1	−683.450801 (−17.8)	−682.455404 (−19.0)	−19.9
TSP$_1$P$_{17}$ + NO	8.2	−683.390087 (20.3)	−682.401210 (15.0)	7.4
TSP$_3$P$_{10}$ + N$_2$	12.6	−683.581103 (99.5)	−682.590651 (−103.9)	−105.3

[a] The calculated results at the HF/6-31G(d,p) level. [b] The calculated results at the MP2/6-31G(d,p) level.

competition than **Path1 P$_1$** and **Path P$_2$**. Finally, let us compare the feasibility of **Path1 P$_1$** and **Path P$_2$**. In terms of the relative energies of **TSa$_1$P$_1$** (−26.0) and **TSa$_1$P$_2$** (−28.6), these two pathways may have comparable contribution to the ^{1}CHCl + N$_2$O reaction. On the other hand, since **P$_1$** is 26.9 kcal/mol higher than **P$_2$**, the formation of **P$_2$** is thermodynamically more favorable than **P$_1$**. Thus, the actual yields of these two products may depend on the reaction conditional in the experiment.

As a result, reflected in final product distributions, we predict that (1) a total of three kinds of products **P$_{16}$** NO + HCN + Cl, **P$_{10}$** N$_2$ + HCl + CO, and **P$_4$** ClCN + HNO should be observed; (2) **P$_{16}$** is the most favorable product with a considerably large yield; (3) **P$_{10}$** should be the second feasible product; (4) **P$_4$** is the least competitive product.

3.4 Experimental Implications. The initial step in four feasible reaction pathways above-mentioned is a barrier-consumed end-N association process with a moderate barrier of 8.9 kcal/mol at the QCISD(T)/6-311G(d,p)//B3LYP/6-31G(d,p) + ZPE level. By means of our calculated potential energy surface, we roughly estimate the theoretical rate constant of the

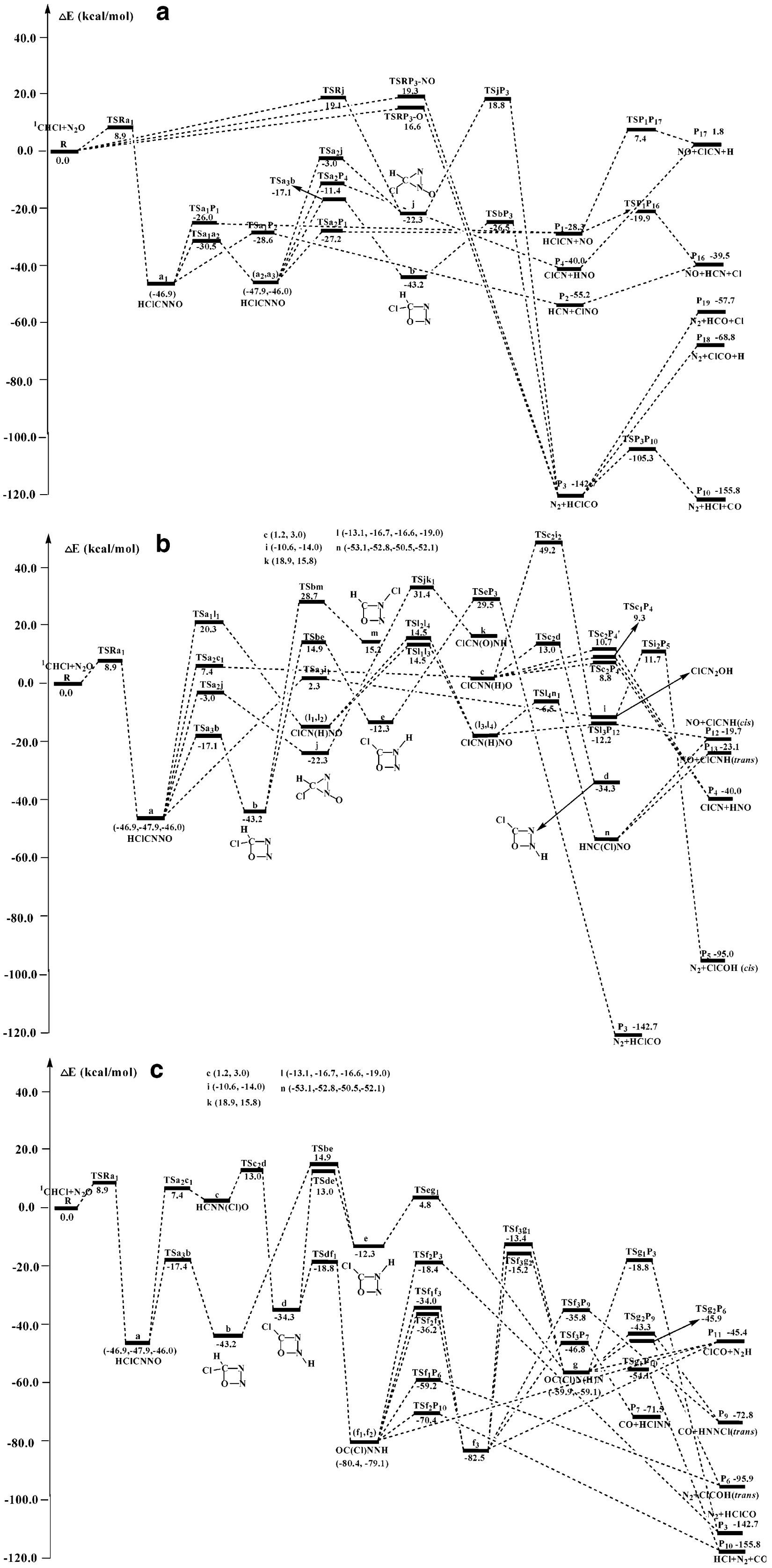

Figure 4. **(a)** Potential energy surface of the relevant reaction pathways for the ^{1}CHCl + N_2O reaction at the QCISD(T)/6-311G(d,p)//B3LYP/6-31G(d,p) + ZPE level. **(b)** The potential energy surface of the unfeasible reaction channels for the ^{1}CHCl + N_2O reaction at the QCISD(T)/6-311G(d,p)//B3LYP/6-31G(d,p) + ZPE level. **(c)** The potential energy surface of the unfeasible reaction channels for the ^{1}CHCl + N_2O reaction at the QCISD(T)/6-311G(d,p)//B3LYP/6-31G(d,p) + ZPE level.

initial step, i.e., ^{1}CHCl + N_2O **R**→HFCNNO **a$_1$** based on the simple transition state theory. The rate constant formula $k = KT/h\ e^{\Delta S/R}e^{-\Delta E/RT}$ is used, where k, ΔS, ΔE denotes the rate constant, entropy difference, and barrier height, respectively. On the basis of the calculated values $\Delta S = -0.031937$ kcal·mol^{-1}.K^{-1}, $\Delta E = 8.9$ kcal·mol^{-1}, we can obtain the rate constant 2.77×10^{-19} cm^{3}molecule^{-1}s^{-1} at $T = 295$ K for the title reaction. It should be pointed out that once such a high-energy transition state **TSRa$_1$** is surmounted, the title reaction will enter the potential well with about 46.9 kcal/mol energy and subsequently some important reaction pathways lies below the reactants **R**. As a consequence, we expect that **TSRa$_1$** is the rate-determining transition state for the total reaction and the calculated rate constant 2.77×10^{-19} cm^{3}molecule^{-1}s^{-1} can represent roughly the low reactivity of the title reaction. However, the experimental and theoretical rate constants are not obtained as yet. Since the title reaction may be important in high-temperature processes, it is very desirable to perform experimental measurements on the high-temperature rate constants for the title reaction in future.

On the other hand, it should be pointed out that the most favorable product **P$_{16}$** $NO + HCN + Cl$ involves two pollutants NO and Cl which are expected to be reduced at all times. So, the title reaction should escape to take place in the atmosphere. To understand the title reaction, it is desired to perform laboratory investigations on the product distribution ratio and reaction rate constant for the title reaction.

3.5 Comparison with the $^1CH_2 + N_2O$ and $^1CHF + N_2O$ Reactions. It is of interest to compare the potential energy surface feature of the title $^1CHCl + N_2O$ reaction with those of the analogous ones $^1CH_2 + N_2O$ and $^1CHF + N_2O$. Recently, we studied in detail the singlet PES of the $^1CH_2 + N_2O$[28] and $^1CHF + N_2O$[29] reactions. By comparison, it is readily found that the features of potential energy surfaces on the $CHX + N_2O$ ($X = H$, F, and Cl) reactions are almost in parallel. The reaction pathways leading to the feasible products (including the secondary dissociation pathways) can be summarized as

Path1: $^1CHX + N_2O \rightarrow HXCNNO \rightarrow HXCN + NO \rightarrow HCN + NO + X$ or $XCN + NO + H$

Path2: $^1CHX + N_2O \rightarrow HXCNNO \rightarrow HCN + XNO \rightarrow HCN + NO + X$

Path3: $^1CHX + N_2O \rightarrow HXCNNO \rightarrow XCN + HNO \rightarrow XCN + NO + H$

Path4: $^1CHX + N_2O \rightarrow HXCNNO \rightarrow HX\text{-}c(CNNO) \rightarrow N_2 + HXCO \rightarrow N_2 + CO + HX$ or $N_2 + HCO + X$ or $N2 + XCO + H$

Note that for $^1CH_2 + N_2O$ reaction, **Path2** and **Path3** depict the same reaction process (H-shift). However, some quantitative discrepancy leads to the different product distribution for the three reactions. For the $^1CH_2 + N_2O$ reaction, $HCN + NO + H$ (via **Path1** and **Path2**) and $N_2 + H_2CO$ (via **Path4**) are the most favorable products with a comparable yield. For the $^1CHF + N_2O$ reaction, only four primary products can be obtained because the secondary dissociation products are thermodynamically and kinetically prohibited. The most feasible product is $HFCN + NO$ (via **Path1**), the second feasible products are $N_2 + HFCO$ (via **Path4**) and $HCN + FNO$ (via **Path2**), and the least feasible product is $FCN + HNO$ (via **Path3**). For the title reaction, three products can be formed, i.e., $HCN + NO + Cl$ (via **Path1** and **Path2**), $N_2 + HCl + CO$ (via **Path4**), and $ClCN + HNO$ (via **Path3**). The order of their feasibility should be $HCN + NO + Cl \gg N_2 + HCl + CO > ClCN + HNO$.

As we can see, all these four pathways involve the same end-N association process $^1CHX + N_2O \rightarrow HXCNNO$ ($X = H$, F, Cl). However, it is worthwhile to note that for such a process, the barrier heights of three reactions lie in the distinct difference, i.e., zero-barrier for $^1CH_2 + N_2O$, 13.5-barrier for $^1CHF + N_2O$, and 8.9-barrier for $^1CHCl + N_2O$. First, we can discuss the reactivity of the three reactions in terms of these barrier heights. The decreasing barrier height increases the carbene reactivity from $^1CHF + N_2O$,$^1CHCl + N_2O$ to $^1CH_2 + N_2O$. As a result, the total rate constants of ^1CHX with N_2O reactions are 6.0×10^{-23}, 2.77×10^{-19}, and $(6.3 \pm 0.7) \times 10^{-11}$ cm^{3}molecule^{-1}s^{-1} for $X = F$, Cl, and H, respectively.[29,31] Further, simply based on the Allned−Rochow electronegativity of F (3.91), Cl (3.00), and H (2.20),[32] the change of the barrier heights can be interpreted. Since the electronegativity of Cl lies between these of F and H, the barrier height of the initial end-N association of the $^1CHCl + N_2O$ reaction lies between these of $^1CHF + N_2O$ and $^1CH_2 + N_2O$ reactions. The previous experimental and theoretical studies[8−27] showed that the reactivity of CHX ($X = H$, F, Cl) toward the same species increases with decreasing electronegativity. Our calculated results confirm such a law. Interestingly, although $CHX + NO$ ($X = H$, F, Cl) reaction system follows the same law, no barrier is found in the similar N-end association processes to form HXCNO intermediate.

By comparing that the theoretical results of three reactions $CHX + N_2O$ ($X = H$, F, and Cl), we can find that the other distinct difference is the secondary dissociation of the primary products. For the $^1CH_2 + N_2O$ reaction, the fragments H_2CN (in **Path1**) and HNO (in **Path2**) can further dissociate to form $HCN + H$ and $NO + H$, respectively, whereas the fragment H_2CO is kinetically stable and cannot further dissociate to the small fragments. For the $^1CHF + N_2O$ reaction, all primary products cannot further dissociate because their secondary dissociation products are thermodynamically prohibited. For the $^1CHCl + N_2O$ reaction, the fragments HClCN, ClNO, and HClCO can further dissociate to form $Cl + HCN$, $Cl + NO$, and $HCl + CO$, respectively. Clearly, the feasibility of the secondary dissociation for the fragments HXCN and HXCO is consistent with the decreased C−X bond enthalpies along $X = F$, H and Cl.[33] Such a result may be similar with that of $^1CHX + NO$ (As shown in the Introduction).

On the other hand, it is worthy noticing that for the $^1CH_2 + N_2O$ reaction, a direct abstraction reaction process leading to $N_2 + H_2CO$ may play an important role at high temperatures, whereas for the $^1CHF + N_2O$ and $^1CHCl + N_2O$ reactions, the direct abstraction reaction pathways are not feasible. Clearly, when H-atom is substituted by halogen atom, the attraction interaction between C-atom and O-atom is decreased.

A discussion of the properties of the $^1CHF + N_2O$ and $^1CHCl + N_2O$ reactions on the basis of substitution effect may be useful. We notice that the process $HXCNNO \rightarrow HCN + XNO$ or $XCN + HNO$ (in **Path2** or **Path3**), which can be depicted as a concerted X-shift ($X = H$, F, Cl) and N−N bond cleavage process, plays an important role. For the $^1CHF + N_2O$ reaction, **Path2** is more feasible than **Path3** but less than **Path1**, whereas for the $^1CHCl + N_2O$ reaction, **Path2** is more feasible than **Path3** and may compete with **Path1**. By comparison, we can find a concerted X-shift ($X = F$, Cl) and N−N bond cleavage process prevails to H-shift and N−N bond cleavage process. Further, the Cl-shift and N−N bond cleavage process prevails to the F-shift and N−N bond cleavage process. Therefore, in terms of the concerted X-shift ($X = F$, Cl, Br, I) and N−N bond cleavage, the order of feasibility may be consistent with the decreased electronegativity of halogen atoms.

As an extrapolation, we would like to discuss the other two potentially important reactions of ^{1}CHBr + N_2O and ^{1}CHI + N_2O that have not been previously studied both experimentally and theoretically. According to the difference of electronegativity of halogen atom(F > Cl > Br > I), we predict that the mechanisms of the ^{1}CHBr and ^{1}CHI reactions with N_2O should be more related to the title reaction ^{1}CHCl + N_2O than to ^{1}-CHF + NO. **Path1-Path4** may play significant roles. Moreover, the Allned-Rochow electronegativities of I (2.56) and Br (2.76) are smaller than those of Cl (3.00) and F (3.91), yet are larger than that of H (2.20).[32] Then, in terms of NO, the carbene reactivities of ^{1}CHBr and ^{1}CHI should be higher than those of ^{1}CHCl and ^{1}CHF, and still lower than that of $^3CH_2$. Accordingly, the total rate constants of ^{1}CHBr + N_2O and ^{1}CHI + N_2O reactions are expected to be between that of $^3CH_2$ + NO and those of ^{1}CHCl + NO and ^{1}CHF + NO.

4. Conclusions

A detailed theoretical survey on the singlet potential energy surface of the ^{1}CHCl + N_2O reaction system is performed at the B3LYP and QCISD(T) levels. The main results can be summarized as follows:

(1) In various possible initial association ways, the end-N attack of ^{1}CHCl at N_2O is expected to be the most feasible pathway leading to HClCNNO **a**. Starting from **a**, three kinds of products $\mathbf{P_{16}}$ NO + HCN + Cl, $\mathbf{P_{10}}$ N_2 + HCl + CO, and $\mathbf{P_4}$ ClCN + HNO should be observed. Among these products, $\mathbf{P_{16}}$ is the most favorable product with a considerably large yield, whereas $\mathbf{P_{10}}$ should be the second feasible product followed by $\mathbf{P_4}$ is the least competitive product.

(2) Further comparisons are made on the potential energy surface of the ^{1}CHCl + N_2O reaction with those of the analogous $^1CH_2$ + N_2O and ^{1}CHF + N_2O. For the ^{1}CHX + N_2O reactions, the total rate constants may increase along X = F, Cl, and H with the decreased electronegativity. On the other hand, although the features of their potential energy surfaces are quite in parallel, the corresponding product distributions are different due to the quantitative discrepancy. The order of the dissociation feasibility for two important fragments HXCN and HXCO is consistent with the decreased C−X bond enthalpies along X = F, H, Cl, Br, and I. In addition, in terms of the concerted X-shift (X = F, Cl, Br, and I) and N−N bond cleavage which may play an important role in the ^{1}CHX + N_2O reaction, the order of feasibility may be consistent with the decreased electronegativity of halogen atom.

Acknowledgment. This work is supported by the National Natural Science Foundation of China (Grant Nos. 29892168, 20073014, 20103003).

References and Notes

(1) Wayne, R. P. *Chemistry of the Atomspheres*; Oxford University Press: Oxford, 1985.

(2) Moss, S. J.; Ledwith, A. *The Chemistry of the Semiconductor Industry*, 1986.

(3) Kaye, J. A.; Penkett, S. A.; Ormond. F. M., Eds. *Report on Concentrations, Lifetimes and Trends of CFCs, Halons and Related Species*: NASA Reference Publication #1339, 1994.

(4) *Scientific Assessment of Ozone Depletion*: World Meteorological Organization: Geneva, 1995.

(5) Montzka, S. A.; Butler, J. H.; Myers, R. C.; Thompson, T. M.; Swanson, T. H.; Clarke, A. D.; Lock, L. T.; Elkins, J. W. *Science* **1996**, *272*, 1318.

(6) *Halon Replacements*; Miziolek, A. W., Tsang, W., Eds.; ACS Symp. Ser. 611; American Chemical Society: Washington, DC., 1995.

(7) Haynes, B. S. *Combust. Flame 28*. **1977**, *113*, 81.

(8) Harding, L. B.; Schlegel, H. B.; Krishnan, R.; Pople, J. A., *J. Phys. Chem.* **1980**, *84*, 3394.

(9) Rondan, N. G.; Houk, K. N.; Moss, R. A.; *J. Am. Chem. Soc*. **1980**, *102*, 1770, and references therein.

(10) Cain, S. R.; Hoffman, R.; Grant, E. R. *J. Phys. Chem*. **1981**, *85*, 4046.

(11) Houk, K. N.; Rondan, N. G.; Mareda, J. *J. Am. Chem. Soc*. **1984**, *106*, 4291.

(12) Houk, K. N.; Rondan, N. G.; Mareda, J. *J. Am. Chem. Soc*. **1984**, *106*, 4293.

(13) Sosa, C.; Schlegel, H. B., *J. Am. Chem. Soc*. **1984**, *106*, 5847.

(14) Moreno, M.; Lluch, J. M.; Oliva, A.; Bertran, J., *J. Phys. Chem*. **1988**, *92*, 4180.

(15) Carstensen, H.-H, Rehbein, C.; Wagner, H. Gg., *Ber, Bunsen-Ges. Phys. Chem.* **1997**, *101*, 1429.

(16) Battin-Leclerc, F.; Smith, A. P.; Hayman, G. D.; Murrells, T. P., *J. Chem. Soc., Faraday Trans*. **1996**, *92*, 3305.

(17) Hack, W.; Wagner, M., *J. Phys. Chem.* **1995**, *99*, 10 847.

(18) Cookson, J. L.; Hancock, G..; Mckendrick, K. G., *Ber. Bunsen-Ges. Phys. Chem.* **1985**, *89*, 335.

(19) Edelbüttel-Einhaus, J.; Hoyermann, K.; Rohde, G..; Wagner, H. Gg. *Ber. Bunsen-Ges. Phys. Chem.* **1989**, *93*, 1413.

(20) Wagener, R.; Wagner, H. Gg., *Z. Phys. Chem*. **1992**, *75*, 9.

(21) Baren, R. E.; Erickson, M. A.; Hershberger, J. F., *Int. J. Chem. Kinet.* **2002**, *34*, 12.

(22) Roggenbuck, J.; Temps, F. *Chem. Phys. Letter*. **1998**, *285*, 422.

(23) Shapley, W. A.; Bacskay, G. B. *Ther. Chem. Acc*. **1998**, *100*, 212.

(24) Shapley, W. A.; Bacskay, G. B. *J. Phys. Chem. A* **1999**, *103*, 4505.

(25) Shapley, W. A.; Bacskay, G. B. *J. Phys. Chem. A* **1999**, *103*, 4514.

(26) Liu, J. J.; Ding, Y. H., Feng, J. K.; Sun, C. C., *J. Phys. Chem. A* **2001**, *105*, 9901.

(27) Liu, J. J.; Ding, Y. H., Tao, Y. G.; Feng, J. K.; Sun, C. C. *J. Comput. Chem.* **2002**, *23*, 625.

(28) Liu, J. J.; Feng, J. K.; Ding, Y. H.; Ren, A. M.; Wang, S. F.; Sun, C. C.; Kong, F. A., *J. Phys. Chem.* A **2001**, *105*, 5885.

(29) Liu, J. J.; Ding, Y. H., Feng, J. K.; Sun, C. C., J. Phys. Chem. A, **2002**, *106*, 2695.

(30) Frisch, M. J.; Trucks, G. W.; Schlegel, H. B.; Scuseria, G. E.; Robb, M. A.; Cheeseman, J. R.; Zakrzewski, V. G.; Montgomery, J. A.; Stratmann, Jr., R. E.; Burant, J. C.; Dapprich, S.; Millam, J. M.; Daniels, A. D.; Kudin, K. N.; Strain, M. C.; Farkas, O.; Tomasi, J.; Barone, V.; Cossi, M.; Cammi, R.; Mennucci, B.; Pomelli, C.; Adamo, C.; Clifford, S.; Ochterski, J.; Petersson, G. A.; Ayala, P. Y.; Cui, Q.; Morokuma, K.; Malick, D. K.; Rabuck, A. D.; Raghavachari, K.; Foresman, J. B.; Cioslowski, J.; Ortiz, J. V.; Stefanov, B. B.; Liu, G.;. Liashenko, A.; Piskorz, P.; Komaromi, I.; Gomperts, R.; Martin, R. L.; Fox, D. J.; Keith, T.; Al-Laham, M. A.; Peng, C. Y.; Nanayakkara, A.; Gonzalez, C.; Challacombe, M.; Gill, P. M. W.; Johnson, B.; Chen, M.; Wong, W.; Andres, J. L.; Gonzalez, C.; Head-Gordon, M.; Replogle, E. S. and Pople, J. A., *Gaussian98W*, revision A.7 Gaussian, Inc., Pittsburgh, PA, 1998.

(31) Koch, M.; Temps, F.; Wagener, R.; Wagner, H. Gg. *Ber. Bunsen-Ges., Phys. Chem*. **1990**, *94*, 645.

(32) Cotton, J. A.; Wikinson, G. *Advanced Inorganic Chemistry*, 1972.

(33) Steudel, R. *Chemistry of the Non-Metals*, 1977.